

# Engine Start-Up Robust Control for a Power-Split Hybrid System Based on $\mu$ Synthesis Method

Zhiguo Zhao,<sup>1</sup> Jiaqi Fan,<sup>1</sup> Mengna Li,<sup>1</sup> and Jing Fu<sup>1</sup>

<sup>1</sup>Tongji University, China

## Abstract

Engine starting control is of great importance for the mode transition process from pure electric mode to electronic-Continuously Variable Transmission (e-CVT) mode for an input power-split system. To suppress the impact of engine start-up on the powertrain, and improve the vehicle ride comfort during the mode transition process, this study proposes an engine start-up robust control strategy based on the  $\mu$  synthesis method. Firstly, the models of powertrain dynamics and the engine ripple torque (ERT) are established, and the mode transition process is analyzed. Secondly, the engine start-up robust control strategy is proposed to distribute the torque of each power source. The optimal engine cranking speed trajectory is designed based on a dynamic programming algorithm aimed at reducing the engine start-up time and improving the vehicle ride comfort. Finally, to track the optimal engine speed trajectory and the desired power output-end speed, a robust controller is developed based on the  $\mu$  synthesis method, which considers the system's parametric perturbations and external disturbances. Simulation results on the MATLAB/Simulink platform indicate that the proposed approach can effectively reduce the vehicle longitudinal jerk during the engine starting process and possess superior robust performance against parametric perturbations and external disturbances.

## History

Received: 26 Apr 2020  
Revised: 28 Jul 2020  
Accepted: 14 Dec 2020  
e-Available: 27 Apr 2021

## Keywords

Input power-split system, Engine start-up, Dynamic programming, Robust control,  $\mu$  synthesis

## Citation

Zhao, Z., Fan, J., Li, M., and Fu, J., "Engine Start-Up Robust Control for a Power-Split Hybrid System Based on  $\mu$  Synthesis Method," *SAE Int. J. Elect. Veh.*, 10(1):89-101, 2021, doi:10.4271/14-10-01-0007.

ISSN: 2691-3747  
e-ISSN: 2691-3755



## Introduction

**D**ue to issues of environmental pollution and energy crisis, hybrid electric vehicles (HEVs) are drawing more and more attention, and the power-split hybrid system is regarded as one of the most promising configurations for HEVs [1, 2]. A power-split hybrid transmission can connect the motor/generator to the engine through planetary gear sets to perform the electronic-Continuously Variable Transmission (e-CVT) hybrid drive mode [3]. In the e-CVT mode, the engine can always work in the optimal operating range, which could significantly optimize the vehicle fuel economy and reduce carbon emissions [4]. However, the unsatisfactory ride comfort for power-split HEVs remains a problem, especially during the mode transition process from electric mode to e-CVT mode. As the engine shaft is directly coupled to the powertrain through planetary gear sets, the engine ripple torque (ERT) during engine start-up would cause intense fluctuations in the powertrain, which results in significant longitudinal jerk to the vehicle [5, 6].

Studies have been carried out to achieve good performance of engine start-up. Su et al. [7] established an ERT model based on the theoretical formula and experimental data. Zhuang et al. [8] utilized a dynamic programming algorithm to solve optimal engine speed trajectory, aimed at ensuring vehicle power performance and reducing engine starting time. Further, Zhao et al. [9] designed an optimal engine speed curve considering ride comfort and developed an engine start-up control strategy. However, with feedforward control or proportional-integral-derivative (PID) control, the tracking performance of the optimal speed curve cannot be guaranteed thus the tracking controller needs to be further investigated.

For the HEVs, numerous investigations have been taken to improve the ride comfort during the mode transition process from pure electric mode to e-CVT mode. Hwang et al. [6] applied motor compensation torque to suppress engine torque pulsations. Wang et al. [10] proposed an active damping strategy based on engine torque estimation and wheel speed observation. Further, Li et al. [11] designed a fuzzy control and two-degrees-of-freedom active damping control algorithms to reduce the impact of ERT during the engine starting process. Zeng et al. [12, 13] established a prediction model for the mode switching process and reduced the vehicle jerk by limiting the changing rate of power source torque. Zeng et al. [14] estimated the engine dynamic torque by applying a full-time artificial neural network and proposed a dynamic coordinated control strategy. However, the above control strategies are all model based, which do not adequately consider the influence of model uncertainties. Thus approaches are adopted to ensure robust performance, such as the fuzzy adaptive sliding-mode control [15], the  $H_\infty$  robust coordinated control [16, 17], and the  $\mu$  synthesis robust control [18, 19]. However, these researches mainly focused on the clutch engagement control for a parallel HEV, and the ERT was also neglected. For a power-split system with planetary gear sets, the configuration is more complex, and parameters such as shaft damping

coefficients cannot be accurately measured. In addition, strong external disturbances such as measurement noise and the change of load torque are also inevitable. Therefore, it is necessary to further improve the robustness against parametric perturbations and external disturbances during the engine start-up process.

Therefore, this article presents an optimal engine start-up robust control strategy based on  $\mu$  synthesis and D-K iteration. The comparative study of PID control and  $\mu$  synthesis robust control is implemented via MATLAB/Simulink simulation, and the robust performance is also verified. In addition, the proposed control strategy is not only effective for the engine start-up process but can also be adopted for the engine shutdown process, which provides guidance for the development of the coordinated control for the power-split system.

## Dynamic Modelling and Analysis of Input Power-Split Hybrid System

A self-developed input power-split hybrid system is investigated in this article, and its configuration is shown in Figure 1. The system consists of a diesel engine, an integrated starter and generator (ISG), a torque motor (TM), a single planetary gear, and a two-speed automated manual transmission (AMT). The engine is connected to the planet carrier C, the ISG is connected to the sun gear  $S_1$ , the ring gear R is connected to the output shaft, and the TM is connected to the output shaft through the AMT. The wet brake B is used to lock the ISG in the high-speed power-split mode to prevent electric power cycling. The three main operation modes of the system and the working status of each component are shown in Table 1.

## Powertrain Dynamics Model

While this study mainly focused on the mode transition process of the power-split system from pure electric mode to

**FIGURE 1** Configuration of the power-split system.

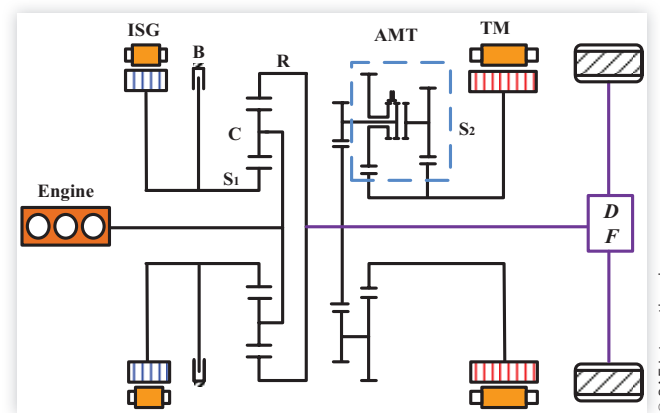


**TABLE 1** The main operation modes of the power-split system.

Operation mode	Engine	ISG	TM	Brake
Pure electric mode	○	○	●	○
E-CVT mode	●	●	●	○
Parallel mode	●	○	●	●

○ off/● on.

e-CVT mode, the brake actuation can be ignored, and the two-speed AMT can be seen as a fixed speed ratio transmission. In this study, the second gear ratio of ATM is used for the model. To simplify the model establishment, the damping coefficients of the two motor shafts are neglected, since they are relatively small compared to the engine shaft and the output shaft. A dynamics model of the power-split system is built, which considers the damping of the engine shaft and the output shaft, and integrates the moment of inertia of each gear into the component to which it is connected. The powertrain kinetic equations are as follows:

$$T_{S1} = T_{ISG} - J_{ISG}\dot{\omega}_{ISG} \quad \text{Eq. (1)}$$

$$T_{S2} = T_{TM} - J_{TM}\dot{\omega}_{TM} \quad \text{Eq. (2)}$$

$$T_C = T_{ENG} - J_{ENG}\dot{\omega}_{ENG} - c_{ENG}\omega_{ENG} \quad \text{Eq. (3)}$$

$$T_L = T_R - J_L\dot{\omega}_L - c_L\omega_L \quad \text{Eq. (4)}$$

where  $T$ ,  $J$ ,  $\omega$ , and  $c$  represent the torque, moment of inertia, angular velocity, and damping coefficient, respectively. ENG and L represent the engine and the equivalent load of the output, respectively. C, R, S<sub>1</sub>, and S<sub>2</sub> represent the planet carrier, the ring gear, the sun gear, and the gear connecting the AMT and the TM, respectively.

The torque balance equations of the transmission system are as follows:

$$(i_1 + 1)T_{S1} + T_C = 0 \quad \text{Eq. (5)}$$

$$i_1 T_{S1} - i_2 T_{S2} = T_R \quad \text{Eq. (6)}$$

where  $i_1$  and  $i_2$  represent the gear ratios of the planetary gear and the AMT, respectively.

According to a kinematics analysis, the relationships of the angular accelerations are as follows:

$$\dot{\omega}_{S1} = (1 + i_1)\dot{\omega}_C - i_1\dot{\omega}_R \quad \text{Eq. (7)}$$

$$\dot{\omega}_{S2} = i_2\dot{\omega}_R \quad \text{Eq. (8)}$$

$$\dot{\omega}_{ISG} = (1 + i_1)\dot{\omega}_{ENG} - i_1\dot{\omega}_L \quad \text{Eq. (9)}$$

$$\dot{\omega}_{TM} = i_2\dot{\omega}_L \quad \text{Eq. (10)}$$

**FIGURE 2** Test bench for ERT.



## ERT Model

For the researched power-split system, the ERT during the engine starting process acts straight on the powertrain. Therefore, to fully reflect the system dynamic characteristics, an ERT model is established combining the experimental data and theoretical formula [9, 10]. The test bench for ERT is shown in Figure 2. Based on the ERT model, the ERT curves shown in Figure 3 are obtained, which are related to the engine crank angle and the engine speed.

## Mode Transition Process Analysis

The lever diagram of the power-split system is shown in Figure 4, and the transition process from pure electric mode to e-CVT mode is analyzed. According to Figure 4(a), the vehicle is initially operating in a pure electric mode, which is driven solely by the TM. When there is a need to switch to the e-CVT mode, the ISG starts to output torque to overcome the ERT, which allows the engine to crank to the target speed rapidly. Meanwhile, additional compensation torque is provided by the TM to avoid the decline of the output torque

**FIGURE 3** ERT.

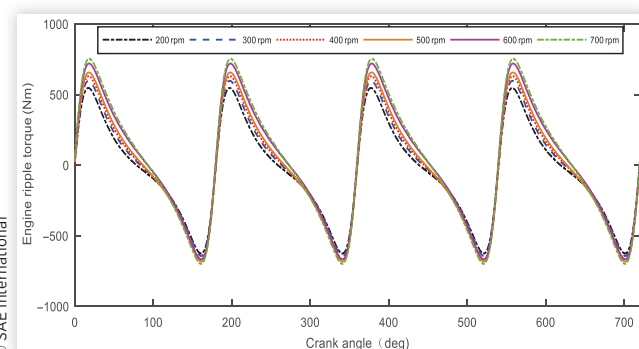
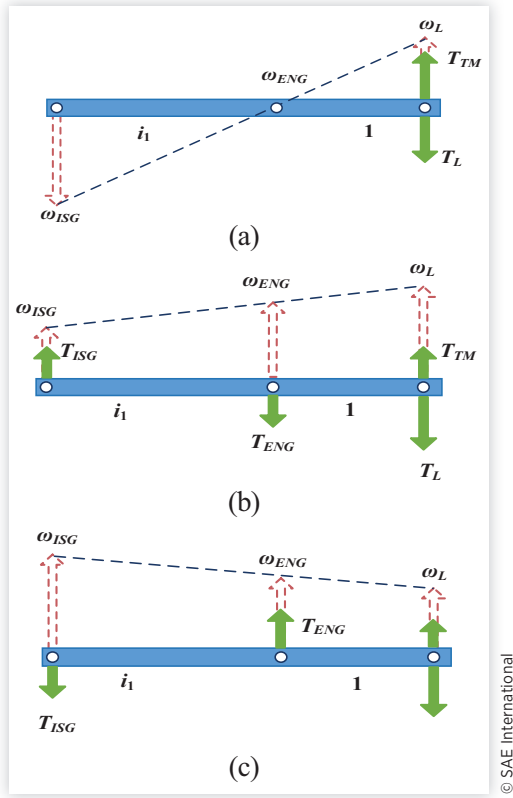


**FIGURE 4** Lever diagram of the mode transition process: (a) Pure electric mode, (b) Engine start-up, (c) e-CVT mode.



© SAE International

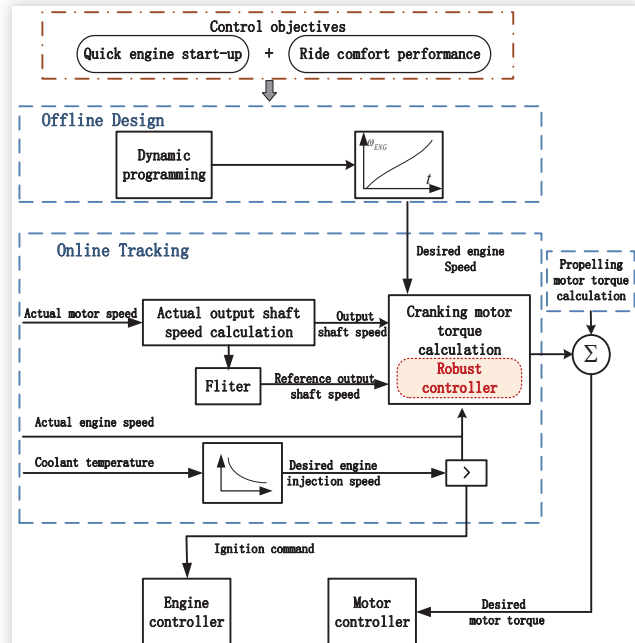
during mode transition. Once the engine speed reaches the desired ignition speed, fuel is injected and ignited, and the engine starts to output the power required by the Vehicle Control Unit (VCU). Finally, the mode transition completes, and the vehicle works in e-CVT mode, as shown in Figure 4(c).

## Engine Start-Up Robust Control Strategy

To reduce the longitudinal jerk caused by the engine start-up during the mode transition process, an engine start-up robust control strategy based on  $\mu$  synthesis is developed, as illustrated in Figure 5. The control objectives are to quickly drag the engine speed to the target speed and to improve the ride comfort during mode transition by coordinating the motor torques.

The control strategy consists of two parts: the offline design of optimal engine speed trajectory and the online tracking of the desired speed. Firstly, the optimal engine speed trajectory is designed based on dynamic programming, which takes into account the ride comfort and engine start-up time. Secondly, in order to track the optimal engine speed trajectory and the desired speed of the output shaft, while considering the parametric perturbations and external disturbances, an

**FIGURE 5** Engine start-up robust control strategy based on  $\mu$  synthesis.



© SAE International

engine start-up robust controller is designed based on  $\mu$  synthesis and D-K iteration. Then the cranking torque of ISG and TM can be calculated and acted on the system, and the engine speed keeps increasing until it reaches the desired ignition speed. The engine begins to work after the engine controller gives the ignition command.

In addition, the propelling torque calculation strategy [10] is also applied in this control strategy, which is used to calculate the motor torque to propel the vehicle during the mode transition process, therefore ensuring the vehicle's power performance.

## Design of Optimal Engine Speed Trajectory

During the engine start-up process, the engine should be dragged to the desired speed as soon as possible while ensuring the best ride comfort. Therefore, the cost function is written as follows:

$$J = \lambda_1 \int_0^T \dot{\omega}_L^4(t) dt + \lambda_2 \int_0^T dt \quad \text{Eq. (11)}$$

where  $\lambda_1$  and  $\lambda_2$  represent the weight coefficients.

In the cost function (Equation 11), the first term indicates the Vibration Dose Value (VDV) in the process of engine start-up, which is the evaluation index of the longitudinal vehicle jerk. The second term represents the engine cracking time.

In addition, the motor torque should meet the following constraints:

$$T_{ISG\min} \leq T_{ISG} \leq T_{ISG\max} \quad \text{Eq. (12)}$$

$$T_{TM\min} \leq T_{TM} \leq T_{TM\max} \quad \text{Eq. (13)}$$

where  $T_{ISG\min}$ ,  $T_{ISG\max}$ ,  $T_{TM\min}$ , and  $T_{TM\max}$  represent the minimal and maximal allowable torques of ISG and TM, respectively.

Based on Equations 1-10, the dynamic equations of the ISG shaft and the TM shaft can be derived as follows:

$$T_{ISG} = \frac{J_1}{(1+i_1)} \dot{\omega}_{ENG} + \frac{J_2}{(1+i_1)} \dot{\omega}_L + \frac{c_{ENG}}{(1+i_1)} \omega_{ENG} - \frac{1}{(1+i_1)} T_{ENG} \quad \text{Eq. (14)}$$

$$T_{TM} = \left( \frac{i_1 J_1}{(1+i_1) i_2} + \frac{J_3}{i_2} \right) \dot{\omega}_{ENG} + \left( \frac{i_1 J_2}{(1+i_1) i_2} + \frac{J_4}{i_2} \right) \dot{\omega}_L + \dots \quad \text{Eq. (15)}$$

$$+ \frac{i_1 c_{ENG}}{(1+i_1) i_2} \omega_{ENG} - \frac{c_L}{i_2} \omega_L - \frac{i_1}{(1+i_1) i_2} T_{ENG} - \frac{1}{i_2} T_L$$

where

$$J_1 = J_{ENG} + (i_1 + 1)^2 J_{ISG}$$

$$J_2 = -i_1(i_1 + 1) J_{ISG}$$

$$J_3 = -i_1(i_1 + 1) J_{TM}$$

$$J_4 = i_1^2 J_{ISG} + i_2^2 J_{TM} + J_L$$

According to Equations 14 and 15, the dynamic equations of the angular acceleration of the engine shaft and the output shaft can be derived as

$$\dot{\omega}_{ENG} = -e_3 c_{ENG} \omega_{ENG} + e_4 c_L \omega_L + e_1 T_{ISG} + e_2 T_{TM} + e_3 T_{ENG} + e_4 T_L \quad \text{Eq. (16)}$$

$$\dot{\omega}_L = -l_3 c_{ENG} \omega_{ENG} + l_4 c_L \omega_L + l_1 T_{ISG} + l_2 T_{TM} + l_3 T_{ENG} + l_4 T_L \quad \text{Eq. (17)}$$

where

$$e_1 = [i_1 J_2 + (i_1 + 1) J_4] / (J_1 J_4 - J_2 J_3)$$

$$e_2 = -i_2 J_2 / (J_1 J_4 - J_2 J_3)$$

$$e_3 = J_4 / (J_1 J_4 - J_2 J_3)$$

$$e_4 = -J_2 / (J_1 J_4 - J_2 J_3)$$

$$l_1 = -[i_1 J_1 + (1+i_1) J_3] / (J_1 J_4 - J_2 J_3)$$

$$l_2 = i_2 J_1 / (J_1 J_4 - J_2 J_3)$$

$$l_3 = -J_3 / (J_1 J_4 - J_2 J_3)$$

$$l_4 = J_1 / (J_1 J_4 - J_2 J_3)$$

Equations 16 and 17 suggest that, during the engine start-up, the ISG and TM work collaboratively to overcome the ERT and the equivalent output load torque, which enable the engine shaft to generate angular acceleration and start to rotate. While the engine start-up process is short, the equivalent

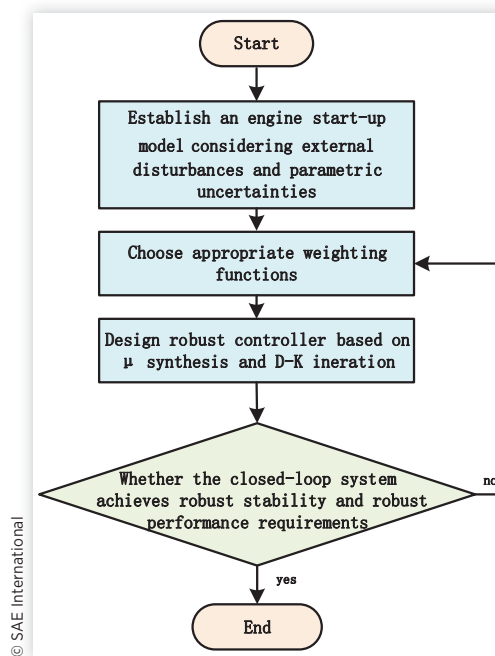
output load torque is considered as a constant value, and the ERT is obtained from the ERT model. The engine speed  $\omega_{ENG}$  and crank angle  $\alpha$  are chosen as the system state variables, and the ISG torque and the TM torque are the control variables. In order to minimize the cost function, a dynamic programming algorithm is applied to obtain the optimal engine speed trajectory from the engine initial state  $(0, \alpha_{initial})$  to the final state  $(\omega_{ENG\_idle}, \alpha_{final})$  [9],  $\alpha_{initial}, \alpha_{final} \in (0^\circ, 720^\circ)$ .

## Design of Engine Start-Up Robust Controller

In most cases, the nominal model could reflect the actual system dynamics of the power-split system. However, some uncertainties would show in the model in practice, such as uncertainties in model parameters or external disturbances, which would highly affect the control accuracy. Thus it is necessary to design a controller that has good robust performance against parametric perturbations and external disturbances. Therefore a robust controller utilizing  $\mu$  synthesis approach is designed in this section. As shown in Figure 6, the design procedure consists of the following steps:

- Step 1: Establish an engine start-up model considering external disturbances and parametric uncertainties.
- Step 2: Choose appropriate weighting functions.
- Step 3: Design the robust controller based on  $\mu$  synthesis and D-K iteration.
- Step 4: If the robust controller achieves robust stability and robust performance requirements, the design process completes; otherwise, return to Step 2.

**FIGURE 6** Flow diagram of the robust controller design.



**Engine Start-Up Model** During the engine start-up process, the ERT varies drastically. Therefore it is challenging to measure or estimate the ERT accurately in real time. Besides, since the external driving conditions of HEVs are complicated, the load torque may not remain at a constant value, which should be treated as a disturbance in the controller design procedure. Furthermore, external disturbances such as measurement noise of the speed sensor are also inevitable. Therefore, considering the disturbances of the ERT, load torque, and the measurement noise, a model for the engine start-up process is built, which lays the foundation for the development of the robust controller [20].

Combining Equations 16 and 17, the dynamical equations can be written in the state-space form:

$$\begin{cases} \dot{x} = Ax + B_1 w + B_2 u \\ z = C_1 x + D_1 u \\ y = C_2 x \end{cases} \quad \text{Eq. (18)}$$

where  $y$  and  $z$  represent the measurement output vector and the performance output vector, respectively. The state vector  $x$ , the control input vector  $u$ , and the external disturbance vector  $w$  are given by

$$x = \begin{bmatrix} \omega_{ENG} \\ \omega_{ENG\_ref} - \omega_{ENG} \\ \omega_L \\ \omega_{L\_ref} - \omega_L \end{bmatrix}, u = \begin{bmatrix} T_{ISG} \\ T_{TM} \end{bmatrix}, w = \begin{bmatrix} T_{ENG} \\ T_L \\ n_{noise} \end{bmatrix}$$

$\omega_{ENG\_ref}$  represents the optimal engine speed trajectory and  $\omega_{L\_ref}$  represents the reference output shaft speed, which is obtained by filtering the actual output shaft speed, to ensure that the output shaft speed changes smoothly.

The parameter matrices  $A$ ,  $B_1$ ,  $B_2$ ,  $C_1$ ,  $C_2$ , and  $D_1$  are written as follows:

$$A = \begin{bmatrix} -e_3 c_{ENG} & 0 & e_4 c_L & 0 \\ e_3 c_{ENG} & 0 & -e_4 c_L & 0 \\ -l_3 c_{ENG} & 0 & l_4 c_L & 0 \\ l_3 c_{ENG} & 0 & -l_4 c_L & 0 \end{bmatrix}, B_1 = \begin{bmatrix} e_3 & e_4 & 0 \\ -e_3 & -e_4 & 1 \\ l_3 & l_4 & 0 \\ -l_3 & -l_4 & 1 \end{bmatrix},$$

$$B_2 = \begin{bmatrix} e_1 & e_2 \\ -e_1 & -e_2 \\ l_1 & l_2 \\ -l_1 & -l_2 \end{bmatrix}$$

$$C_1 = \begin{bmatrix} 0 & 1 & 0 & 0 \\ 0 & 0 & 0 & 1 \\ 0 & 0 & 0 & 0 \\ 0 & 0 & 0 & 0 \end{bmatrix}, D_1 = \begin{bmatrix} 0 & 0 \\ 0 & 0 \\ 1 & 0 \\ 0 & 1 \end{bmatrix}, C_2 = \begin{bmatrix} 0 & 1 & 0 & 0 \\ 0 & 0 & 0 & 1 \end{bmatrix}$$

The damping coefficient of the engine shaft and output shaft cannot be measured accurately and are usually not constant at all times; thus they are described by nominal values and perturbation ranges as follows:

$$\begin{cases} c_{ENG} = \bar{c}_{ENG} (1 + d_{ENG} \delta_{ENG}), & \|\delta_{ENG}\| \leq 1 \\ c_L = \bar{c}_L (1 + d_L \delta_L), & \|\delta_L\| \leq 1 \end{cases} \quad \text{Eq. (19)}$$

where  $\bar{c}$  represents the nominal coefficient value,  $d$  represents the maximum relative uncertainty, and  $\delta$  represents the relative variation in the parameter.

Based on the  $\mu$  synthesis method, parameters are represented in the form of an upper linear fractional transformation (LFT), as shown in

$$\begin{cases} c_{ENG} = F_u \left( \begin{bmatrix} 0 & \bar{c}_{ENG} \\ d_{ENG} & \bar{c}_{ENG} \end{bmatrix}, \delta_{ENG} \right) = F_u(M_{c_{ENG}}, \delta_{ENG}) \\ c_L = F_u \left( \begin{bmatrix} 0 & \bar{c}_L \\ d_L & \bar{c}_L \end{bmatrix}, \delta_L \right) = F_u(M_{c_L}, \delta_L) \end{cases} \quad \text{Eq. (20)}$$

Because the model uncertainty caused by system parameter perturbations has a known structure, it is called structural uncertainty  $\Delta_c$  and is defined as

$$\Delta_c = \text{diag}[\delta_{ENG}, \delta_L] \quad \text{Eq. (21)}$$

In addition, the CAN communication from the vehicle controller to the motor controller introduces time delays to the system, and the motor response also has an inevitable delay. There is also an error between the actual motor torque and the target motor torque, especially in high-frequency domains. Those unmodelled dynamic errors in the control system are treated as nonstructural uncertainty, and a nonstructural uncertainty  $\Delta_{um}$  is introduced. By combining the structural uncertainty  $\Delta_c$  and the nonstructural uncertainty  $\Delta_{um}$ , a new uncertainty  $\Delta$  can be defined as

$$\Delta = \text{diag}[\Delta_c, \Delta_{um}], \quad \|\Delta\|_\infty < 1 \quad \text{Eq. (22)}$$

Based on the plant dynamics represented in Equation 18 and parameter uncertainties represented in Equation 22, a perturbed plant model  $G$  with parameter uncertainties can be obtained in the form of an upper LFT as follows:

$$G = F_u(G_{nom}, \Delta) \quad \text{Eq. (23)}$$

where  $G_{nom}$  is the nominal model.

**Weighting Functions** In this section, appropriate weighting functions are chosen to achieve the desired robust performance.

Three input weighting functions are expressed in Equation 24. The magnitude of the ERT disturbance and the load torque disturbance are scaled by the weighting functions  $W_{T\_ENG}$  and  $W_{T\_L}$ , respectively. The weighting function  $W_n$  is a high-pass transfer function that models the high-frequency white noise.

$$\begin{cases} W_{T\_ENG} = T_{ENG\_max} \\ W_{T\_L} = T_{L\_max} \\ W_n = 10^{-5} \frac{0.1s+1}{0.001s+1} \end{cases} \quad \text{Eq. (24)}$$

where  $T_{ENG\_max}$  and  $T_{L\_max}$  represent the maximum disturbance of the ERT and the load torque, respectively.  $s$  represents the Laplace operator.

The magnitude ISG torque and TM torque are scaled by the weighting function  $W_u$ , which is expressed as

$$W_u = \text{diag} \left[ \frac{1}{T_{ISG\_max}}, \frac{1}{T_{TM\_max}} \right] \quad \text{Eq. (25)}$$

where  $T_{ISG\_max}$  and  $T_{TM\_max}$  represent the maximum ISG torque and the maximum TM torque during the engine start-up process, respectively.

The performance weighting function  $W_e$  reflects the tracking performance, which is constructed as

$$W_e = \text{diag} \left[ \frac{1}{e_{ENG\_max}}, \frac{1}{e_{L\_max}} \right] \quad \text{Eq. (26)}$$

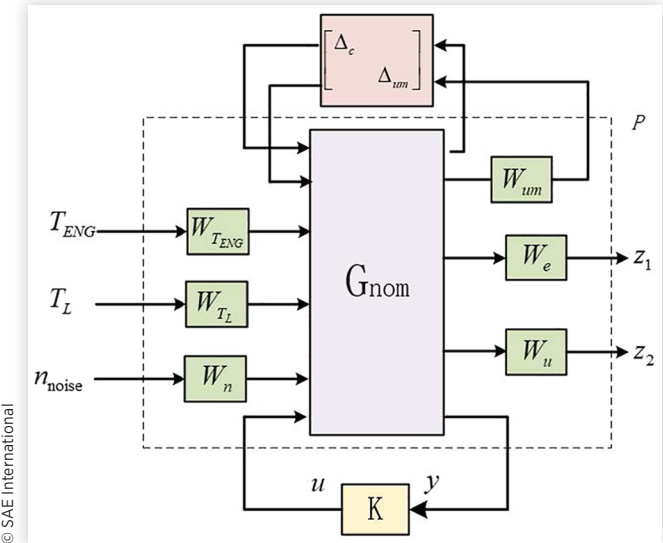
where  $e_{ENG\_max}$  and  $e_{L\_max}$  represent the maximum engine speed tracking error and the maximum output shaft speed tracking error, respectively.

The weighting function  $W_{um}$  reflects the unmodelled error in a specific frequency domain, mainly in the high-frequency part, and is given in Equation 27. The unmodelled error in the low-frequency domain is 4%, and the unmodelled error in the high-frequency domain reaches 100%.

$$W_{um} = \text{diag} \left[ \frac{s+2}{20s+50}, \frac{s+2}{20s+50} \right] \quad \text{Eq. (27)}$$

**Robust Controller Design** The robust control closed-loop system of the engine start-up process is shown in Figure 7. The system mainly consists of the nominal model  $G_{nom}$ , the uncertainty  $\Delta$ , the controller  $K$ , and the weighting functions. The input of the controller  $K$  is the system output vector  $y$ , and the output of the controller  $K$  is the feedback motor torque

**FIGURE 7** Robust control closed-loop system of the engine start-up process.

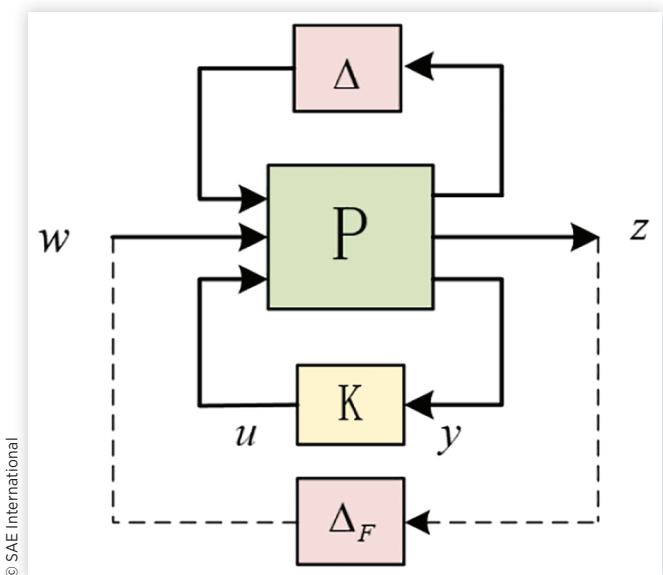


command  $u$ . For convenience, the open-loop system  $P$  is introduced to represent the nominal model with weighting functions. The generalized system of the engine start-up process is displayed in Figure 8.

For robust performance analysis, a block structure of uncertainty  $\Delta_p$  is defined as

$$\Delta_p \in \Delta_p := \left\{ \begin{bmatrix} \Delta & 0 \\ 0 & \Delta_F \end{bmatrix} : \Delta \in R^{4 \times 4}, \Delta_F \in C^{3 \times 4} \right\}, \quad \|\Delta_F\|_\infty \leq 1 \quad \text{Eq. (28)}$$

**FIGURE 8** Generalized system of the engine start-up process.



The first uncertainty  $\Delta$  is used to describe the parametric perturbations, and the second uncertainty  $\Delta_F$  is a fictitious uncertainty, which is introduced to represent the robust performance requirement. The inputs to  $\Delta_F$  are the system performance output vector  $z$ , and the output from  $\Delta_F$  is the external disturbance vector  $w$ .

The design objective of the robust control is that the closed-loop system shown in Figure 7 can achieve robust performance and robust stability. As a result, it is required to find a stabilizing controller  $K$ , which satisfies the condition described in Equation 29 based on the  $\mu$  synthesis theory.

$$\sup_{\omega \in R} \mu_{\Delta_F} [M(j\omega)] < 1 \quad \text{Eq. (29)}$$

where  $M = F_l(P, K)$  is a lower LFT of  $P$  and  $K$ .

The D-K iteration method is utilized to solve the problem in Equation 29, which is based on solving the following problem [21]:

$$\inf_{K(S)} \sup_{\omega \in R} \inf_{D \in D_{\Delta_P}} \bar{\sigma}[DM(j\omega)D^{-1}] \quad \text{Eq. (30)}$$

where  $D_{\Delta_P}$  is the set of matrices that follow  $D\Delta_P = \Delta_P D$  for any  $D \in D_{\Delta_P}$  and  $\Delta_P \in \Delta_p$ .

The D-K iteration problem can be solved with the help of the  $\mu$  synthesis toolbox in MATLAB.

Finally, the cranking torque of ISG and TM can be calculated by the robust controller as follows:

$$u = Ky \quad \text{Eq. (31)}$$

## Simulations and Discussions

Based on the MATLAB/Simulink platform, an input power-split system model is established, and the engine start-up robust control strategy is validated.

## Verification of the Robust Control Strategy

In order to verify the robust optimal control strategy, a coordinated control strategy for the engine start-up process based on PID is applied as the reference control strategy, which can be designed as follows.

First, a PID controller is designed to track the optimal engine speed. The input to the PID controller is the tracking error between the actual engine speed and the desired engine speed, and the output from the PID controller is the desired angular acceleration of the engine. Then, according to Equations 14 and 15, the cranking torque of ISG and TM can be calculated.

Meanwhile, the active damping strategy in Ref. [10] is also adopted in the control method to further reduce the fluctuation of the output shaft speed and improve the ride comfort.

The simulation results of the two control strategies are shown in Figure 8. The key parameters of the HEV are given in Table 2.

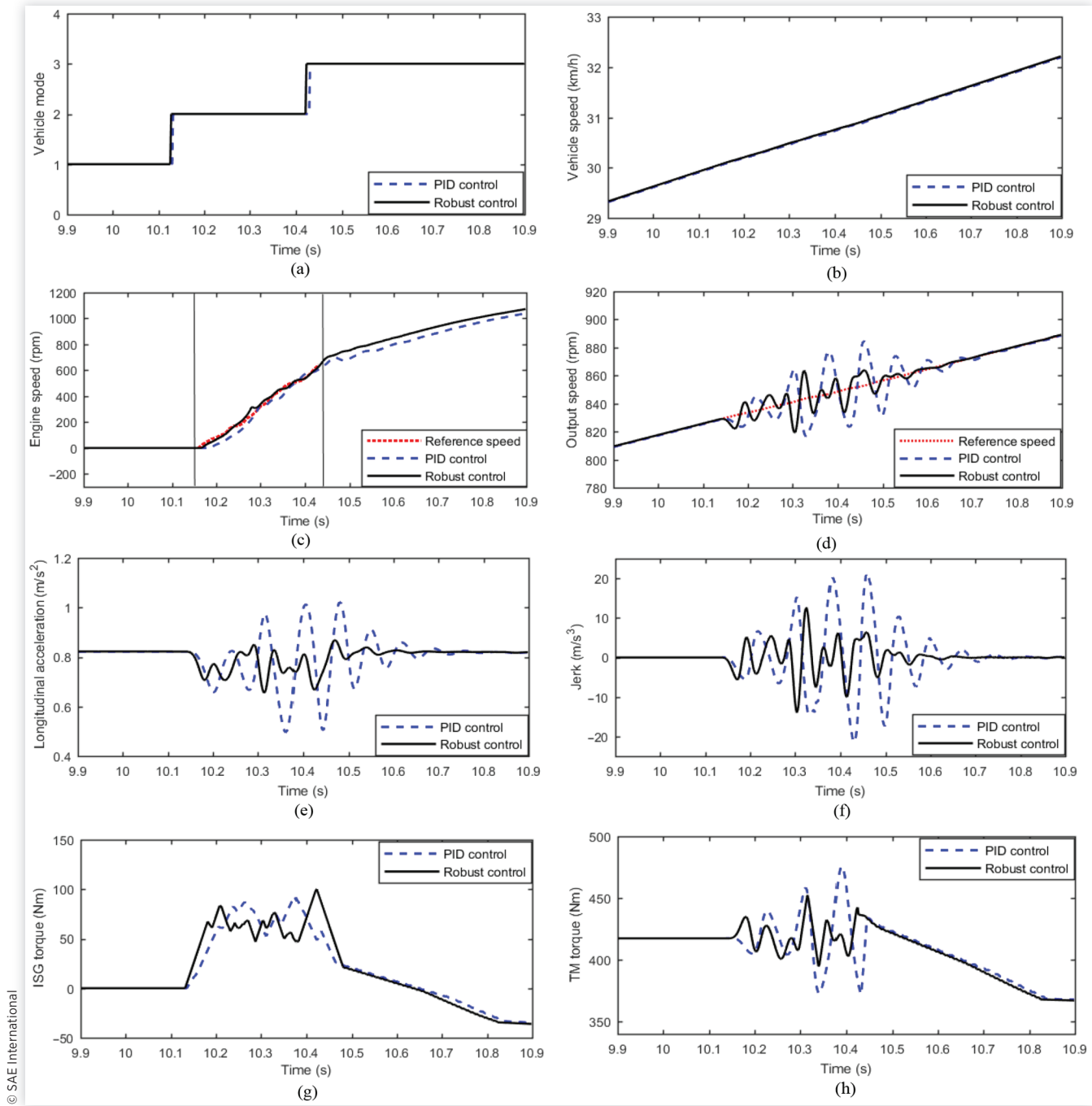
As shown in Figure 9(a), Numbers 1 to 3 indicate the pure electric mode, the engine start-up process, and the e-CVT mode, respectively. The vehicle initially runs in pure electric mode with a constant acceleration, when the vehicle speed reaches 30 km/h, the vehicle begins to switch to the e-CVT mode. The engine start-up process starts at 10.13 s and finishes at 10.43 s with a 0.3 s starting time. It can be seen from the engine speed curve and the vehicle speed curve that with the proposed strategies, the vehicle can successfully complete a quick engine start-up while ensuring the vehicle's power performance.

Figures 9(c) and 9(d) illustrate the engine speed and the output speed of the transmission, which indicates that the designed robust controller achieves a better speed tracking performance than the PID controller. When the PID control strategy is adopted, the output speed increases with relatively large fluctuations, which could transmit to the vehicle wheels and cause a longitudinal impact on the vehicle. As shown

**TABLE 2** Key parameters of HEV.

Parameter	Symbol	Value
Vehicle mass	$m$	16,000 (kg)
Wheel radius	$r_{wh}$	0.47 (m)
Aerodynamics drag coefficient	$C_d$	0.65
Effective frontal area	$A$	7 ( $m^2$ )
Maximum engine torque/speed	$T_{ENGmax}/n_{ENGmax}$	860 (Nm)/2000 (rpm)
Maximum ISG speed	$n_{ISGmax}$	6000 (rpm)
ISG-rated torque/speed	$T_{r\_ISG}/n_{r\_ISG}$	160 (Nm)/3000 (rpm)
Maximum TM speed	$n_{TMmax}$	6000(rpm)
TM-rated torque/speed	$T_{r\_TM}/n_{r\_TM}$	300 (Nm)/2000 (rpm)
Final reduction gear ratio	$i_F$	4.89
Gear ratio of the planetary gear	$i_1$	2.63
Second gear ratio of AMT	$i_2$	2.408
First gear ratio of AMT	$i_3$	6.059
ISG shaft equivalent moment inertia	$J_{ISG}$	0.041 ( $kg \cdot m^2$ )
TM shaft equivalent moment inertia	$J_{TM}$	0.072 ( $kg \cdot m^2$ )
Engine shaft equivalent moment inertia	$J_{ENG}$	0.467 ( $kg \cdot m^2$ )
Output shaft equivalent moment inertia	$J_L$	147.81 ( $kg \cdot m^2$ )
Engine shaft damping coefficient	$c_{ENG}$	0.1 (Nm/(rad/s))
Output shaft equivalent coefficient	$c_L$	0.2 (Nm/(rad/s))

**FIGURE 9** Simulation results during the engine start-up process: (a) Vehicle mode, (b) Vehicle speed, (c) Engine speed, (d) Output speed, (e) Longitudinal acceleration, (f) Longitudinal jerk, (g) ISG torque, (h) TM torque.



in Figures 9(e) and 9(f), the longitudinal acceleration of the vehicle changes sharply between 10.3 s and 10.5 s, and the longitudinal jerk reaches a peak value of  $21.11 \text{ m/s}^3$  at 10.42 s. After optimization with robust control, the fluctuations of the output speed are restrained to a reasonable range within 22 rpm, and the amplitude of the longitudinal jerk reaches a maximum value of  $13.99 \text{ m/s}^3$  at 17.51 s. The maximum amplitude of the longitudinal jerk is effectively reduced by 33.72% compared to the results from the PID control.

## Evaluation of Robust Performance

In this section, the robust performance of the proposed robust control strategy for the engine start-up process is evaluated. The input power-split system is supposed to conduct mode transition under parameter perturbation and external disturbance. The robust performance is evaluated by the following scenarios.

- Case A: The power-split system is regarded as the nominal system without parameter perturbation.
- Case B: The power-split system operates with a +30% damping coefficient perturbation of the engine shaft [22].
- Case C: The power-split system operates with a +30% damping coefficient perturbation of the output shaft.
- Case D: The power-split system operates with an external disturbance of engine speed measurement noise, which is shown in Figure 10.

The simulation results of the four cases are shown in Figure 11, and the associated summaries are given in Table 3.

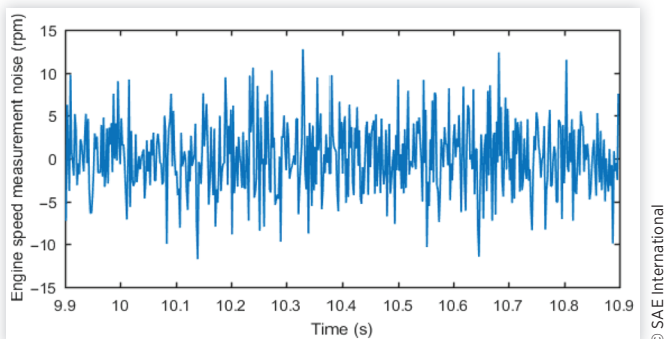
In Case B, the damping coefficient of the engine shaft  $c_{ENG}$  is considered as the uncertain parameter, and the +30% parameter perturbation is added to the simulation system. From Figure 11, it can be observed that the peak amplitude

of the longitudinal jerk is  $13.97 \text{ m/s}^3$ , which is nearly the same as that in Case A. With a +30% damping coefficient perturbation of the output shaft in Case C, the amplitude of the jerk reaches its peak value of  $14.23 \text{ m/s}^3$ , which is only 1.7% higher than that in Case A. In Case D, after adding the measurement noise of engine speed to the system, the maximum amplitude of the jerk is  $14.66 \text{ m/s}^3$ , the control deviation are less than 5% compared to Case A. Vehicle longitudinal acceleration, longitudinal jerk, motor torque, and output speed remain nearly the same as before the parameter perturbation and measurement noise are added. Therefore it can be concluded that the designed robust control strategy has a good robust performance against parameter perturbation and show a particular ability of disturbance attenuation for the external disturbance.

## Conclusion

This study focused on the mode transition process from pure electric mode to the e-CVT mode for an input power-split system. To realize a fast and smooth engine start-up, the engine speed trajectory was designed utilizing the dynamic programming algorithm. In order to track the optimal engine speed trajectory and the desired speed of the output shaft, an engine start-up robust controller was designed based on  $\mu$  synthesis and D-K iteration approaches. The effects of parametric perturbations and external disturbances on the closed-loop system were taken into account in the controller design procedure. The simulation results indicated that, compared to the PID control strategy, the proposed robust control strategy was more effective in reducing the longitudinal jerk and ensuring the ride comfort during the engine start-up process. The robust control also possesses superior robust performance against parametric perturbations and external disturbances. Nevertheless, experiments need to be further implemented to validate these promising results from the proposed approach. Future work could be focusing on the transition process during deceleration from the e-CVT mode to pure electric mode.

**FIGURE 10** Measurement noise of the engine speed sensor.



## Acknowledgments

This study is supported by the National Natural Science Foundation of China (No.51675381). The authors would like to express their sincere thanks for providing the research funding.

## Contact Information

jiaqi\_fanfan@163.com

**FIGURE 11** Simulation results for robust performance evaluation: (a) Vehicle mode, (b) Vehicle speed, (c) Engine speed, (d) Output speed, (e) Longitudinal acceleration, (f) Longitudinal jerk, (g) ISG torque, (h) TM torque.

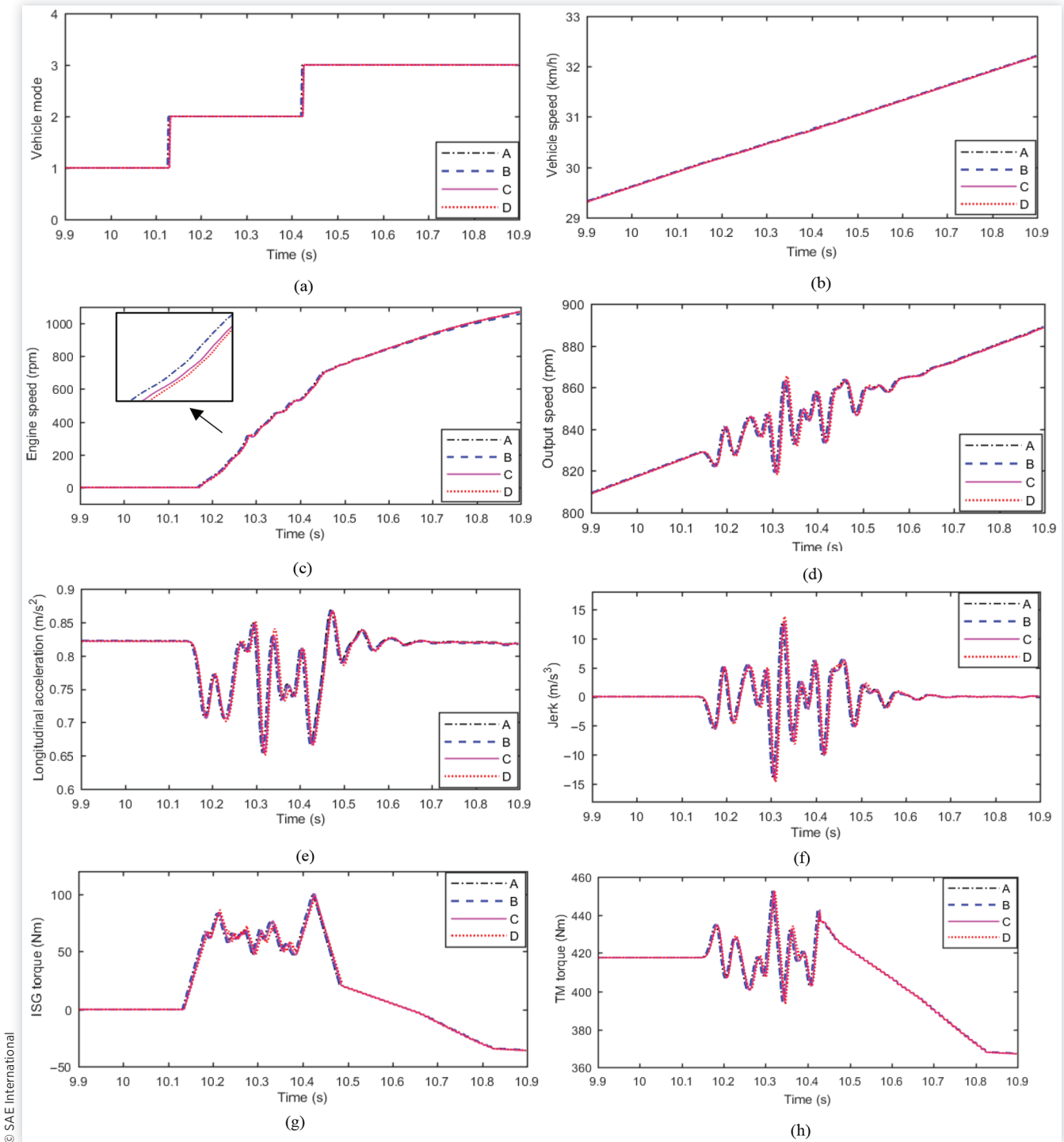


**TABLE 3** Summary of the results.

Case	Longitudinal jerk (m/s <sup>3</sup> )	Control deviation (%)
A	13.99	—
B	13.97	0.1
C	14.23	1.7
D	14.66	4.7

© SAE International

## References

- Wu, G., Zhang, X., and Dong, Z., "Powertrain Architectures of Electrified Vehicles: Review, Classification and Comparison," *Journal of the Franklin Institute* 352, no. 2 (2015): 425-448, doi:10.1016/j.jfranklin.2014.04.018.
- Mashadi, B. and Emadi, S.A.M., "Dual-Mode Power-Split Transmission for Hybrid Electric Vehicles," *IEEE Transactions on Vehicular Technology* 59, no. 7 (2010): 3223-3232, doi:10.1109/tvt.2010.2049870.
- Kim, J., Kim, T., Min, B., Hwang, S. et al., "Mode Control Strategy for a Two-Mode Hybrid Electric Vehicle Using Electrically Variable Transmission (EVT) and Fixed-Gear Mode," *IEEE Transactions on Vehicular Technology* 60, no. 3 (2011): 793-803, doi:10.1109/tvt.2011.2107564.
- Hong, S., Kim, H., and Kim, J., "Motor Control Algorithm for an Optimal Engine Operation of Power Split Hybrid Electric Vehicle," *International Journal of Automotive Technology* 16, no. 1 (2015): 97-105, doi:10.1007/s12239-015-0011-8.
- Liu, D., Yu, H., and Zhang, J., "Multibody Dynamics Analysis for the Coupled Vibrations of a Power Split Hybrid Electric Vehicle during the Engine Start Transition," *Proceedings of the Institution of Mechanical Engineers* 230, no. K4 (2016): 527-540, doi:10.1177/1464419315618862.
- Hwang, H.Y., "Minimizing Seat Track Vibration That Is Caused by the Automatic Start/Stop of an Engine in a Power-Split Hybrid Electric Vehicle," *Journal of Vibration and Acoustics* 135, no. 6 (2013): 061007.1-061007.8, doi:10.1115/1.4023954.
- Su, Y., Hu, M., Su, L., Qin, D. et al., "Dynamic Coordinated Control during Mode Transition Process for a Compound Power-Split Hybrid Electric Vehicle," *Mechanical Systems and Signal Processing* 107, no. July (2018): 221-240, doi:10.1016/j.ymssp.2018.01.023.
- Zhuang, W., Kum, D., Peng, H., Wang, L. et al., "Optimal Engine Starts of an Input-Split Hybrid Electric Vehicle," *SAE Int. J. Alt. Power.* 4, no. 2 (2015): 343-351, doi:<https://doi.org/10.4271/2015-01-1227>.
- Zhao, Z., Jiang, L., Wang, C., and Li, M., "Engine Start-Up Optimal Control for a Compound Power-Split Hybrid Powertrain," *Mechanical Systems and Signal Processing* 120 (2019): 365-377, doi:10.1016/j.ymssp.2018.10.027.
- Wang, C., Zhao, Z., Zhang, T., and Li, M., "Mode Transition Coordinated Control for a Compound Power-Split Hybrid Car," *Mechanical Systems and Signal Processing* 87 (2017): 192-205, doi:10.1016/j.ymssp.2016.10.021.
- Li, M., Zhao, Z., Jiang, L., and Tang, X., "Subsection Coordinated Control during Mode Transition for a Compound Power-Split System," SAE Technical Paper 2019-01-1214, 2019, doi:<https://doi.org/10.4271/2019-01-1214>.
- Zeng, X., Yang, N., Wang, J. et al., "Predictive-Model-Based Dynamic Coordination Control Strategy for Power-Split Hybrid Electric Bus," *Mechanical Systems and Signal Processing* 60-61 (2015): 785-798, doi:10.1016/j.ymssp.2014.12.016.
- Zeng, X. and Wang, J., "Dynamic Coordinated Control Method of Planetary Hybrid Power-Split System," in *Analysis and Design of the Power-Split Device for Hybrid Systems* (Singapore: Springer Singapore, 2018), doi:10.1007/978-981-10-4272-0\_5.
- Zeng, X., Cui, H., Song, D. et al., "Jerk Analysis of a Power-Split Hybrid Electric Vehicle Based on a Data-Driven Vehicle Dynamics Model," *Energies* 11, no. 6 (2018): 1537, doi:10.3390/en11061537.
- Lei, W., "Mode Transition Control for Series-Parallel Hybrid Electric Bus Using Fuzzy Adaptive Sliding Mode Approach," *Journal of Mechanical Engineering* 48, no. 14 (2012): 119, doi:10.3901/JME.2012.14.119.
- Yang, C., Li, L., Jiao, X. et al., "Research on Mode Transition Control for Single-Shaft Parallel Hybrid Powertrain," *Scientia Sinica Technologica* 46, no. 1 (2016): 91-100, doi:10.13140/RG.2.1.4970.6001.
- Yang, C., Jiao, X., Li, L., Zhang, Y. et al., "A Robust H<sub>∞</sub> Control-Based Hierarchical Mode Transition Control System for Plug-In Hybrid Electric Vehicle," *Mechanical Systems and Signal Processing* 99 (2018): 326-344, doi:10.1016/j.ymssp.2017.06.023.
- Zhang, H., Wang, C., Zhang, Y., Liang, J. et al., "Drivability Improvements for a Single-Motor Parallel Hybrid Electric Vehicle Using Robust Controls," *J. Zhejiang Univ.-Sci. A15*, no. 4 (2014): 291-301, doi:10.1631/jzus. A1300356.
- Zhang, H., Zhang, Y., and Yin, C., "Hardware-in-the-Loop Simulation of Robust Mode Transition Control for a Series-

- Parallel Hybrid Electric Vehicle," *IEEE Transactions on Vehicular Technology* 65, no. 3 (2015): 1059-1069, doi:10.1109/TVT.2015.2486558.
20. Zhu, D., Pritchard, E.G.D., and Silverberg, L.M., "A New System Development Framework Driven by a Model-Based Testing Approach Bridged by Information Flow," *IEEE Systems Journal* 12, no. 3 (2016): 2917-2924, doi:10.1109/JSYST.2016.2631142.
21. Hang, P., Chen, X., Luo, F., and Fang, S., "Robust Control of a Four-Wheel-Independent-Steering Electric Vehicle for Path Tracking," *SAE Int. J. Veh. Dyn., Stab., and NVH* 1, no. 2 (2017): 307-316, doi:<https://doi.org/10.4271/2017-01-1584>.
22. Madamedon, M., Gu, F., Aburass, A., and Ball, A.D., "Online Estimation of Engine Driveline Dynamic Response," in *2016 International Conference for Students on Applied Engineering*, Tyne, UK, IEEE, 2016, doi:10.1109/ICSAE.2016.7810216.

